Check for updates

Covalent Organic Frameworks

Zitierweise: Angew. Chem. Int. Ed. 2021, 60, 3727–3736
Internationale Ausgabe: doi.org/10.1002/anie.202013377
Deutsche Ausgabe: doi.org/10.1002/ange.202013377

# Luminescent Ratiometric Thermometers Based on a 4f–3d Grafted Covalent Organic Framework to Locally Measure Temperature Gradients During Catalytic Reactions

*Anna M. Kaczmarek[+],* Himanshu Sekhar Jena[+], Chidharth Krishnaraj, Hannes Rijckaert, Savita K. P. Veerapandian, Andries Meijerink and Pascal Van Der Voort*

**Abstract:** *Covalent Organic Frameworks (COFs), an emerging class of crystalline porous materials, are a new type of support for grafting lanthanide ions ($Ln^{3+}$), which can be employed as ratiometric luminescent thermometers. In this work we have shown that COFs co-grafted with lanthanide ions ($Eu^{3+}$, $Tb^{3+}$) and $Cu^{2+}$ (or potentially other d-metals) can synchronously be employed both as a nanothermometer and catalyst during a chemical reaction. The performance of the thermometer could be tuned by changing the grafted d-metal and solvent environment. As a proof of principle, the Glaser coupling reaction was investigated. We show that temperature can be precisely measured during the course of the catalytic reaction using luminescence thermometry. This concept could be potentially easily extended to other catalytic reactions by grafting other d-metal ions on the Ln@COF platform.*

## Introduction

For the optimal performance of a catalyst—good activity, selectivity as well as stability—certain parameters must be revised.[1] Among them temperature is very important. For example, in chemical reactors temperature inhomogeneities give rise to large variation in reaction yields.[2] So-called traditional thermometers have many intrinsic constraints and are not suitable for temperature measurements of fast moving objects or with resolution at the micron or nanometer scale.[3] Accurate mapping of local temperature fluctuations and variations, even down to the single catalyst particle scale, is the first step towards realizing more homogeneous temperature profiles in catalytic reactors. In order to be able to investigate the local temperature fluctuations, it is crucial to have a non-invasive thermometry technique, with a high spatial and temporal resolution.[4–7] Already various optical methods, such as Raman scattering, thermography, thermal reflection and luminescence have been investigated for use in new types of thermometers.[8] Among these techniques, luminescence-based thermometry is proving to be a very promising alternative for measuring temperature and has shown excellent results in the first studies on in situ luminescence thermometry during catalytic reactions reported by Meijerink and Weckhuysen.[1,2,9–12] Band shape luminescence thermometry is a ratiometric spectroscopic technique, which can be employed to accurately monitor temperature non-invasively.[3] This type of thermometry exploits the changes in the intensity ratio of two (or more) emission peaks with the change of temperature. Up to date, the $Yb^{3+}$-$Er^{3+}$ luminescence system has been dominantly proposed for this purpose. In such a system $Er^{3+}$ is used as the emitting ion and $Yb^{3+}$ is added for efficient upconversion, a process where multiple low-energy photons are used to generate emission of higher energy photons.[13–15] This system is known to show good performance for (high) temperature sensing.[16–22] For example in combination with catalytic applications, microcrystalline $NaYF_4$ doped with $Er^{3+}$ and $Yb^{3+}$ was mixed with a commercial zeolite H-ZSM-5 for investigating the methanol-to-hydrocarbons reaction.[1] Also catalyst $SiO_2$-extrudates carrying Au@$SiO_2$, Rh catalysts and $NaYF_4$:Er,Yb@$SiO_2$ temperature sensors have been reported to simultaneously measure temperature and perform SHINERS (shell-isolated nanoparticle-enhanced Raman spectroscopy) during a Rh-catalyzed CO hydrogenation reaction.[10] It has also been shown that lanthanide-doped $Y_2O_3$ nanoparticles can be deposited onto $\alpha$-$Al_2O_3$, a non-porous catalyst support material.[9] This material could act as both nanothermometer and catalyst, after active catalysts, such as silver or nickel, are co-deposited on the alumina. To extend the temperature range of the nanothermometers different lanthanide dopants were incorporated: $Yb^{3+}$/$Er^{3+}$, $Dy^{3+}$ and $Eu^{3+}$. The high thermal and chemical stability of the $Y_2O_3$ nanoparticles, as well as thermometric behavior of these lanthanides at very high temperatures, makes these materials very promising for sensing in catalytic environments. However, the authors have not tested them in real catalytic reactions. The number of reports on materials, which can simultaneously operate as a nanothermometer and catalyst, is until now very scarce. The up-to-date reported materials consist of a catalytic support or catalyst embedded on the support and separate lanthanide nanoparticles co-deposited

[*] Prof. A. M. Kaczmarek,[+] Dr. H. S. Jena,[+] C. Krishnaraj, Dr. H. Rijckaert, Prof. P. Van Der Voort
Department of Chemistry, Ghent University
Krijgslaan 281-S3, 9000 Ghent (Belgium)
E-Mail: anna.kaczmarek@ugent.be
S. K. P. Veerapandian
Faculty of Engineering and Architecture, Department of Applied Physics
Sint-Pietersnieuwstraat 41 B4, 9000 Ghent (Belgium)
Prof. A. Meijerink
Debye Institute for Nanomaterials Science, Utrecht University
Princetonplein 1, Utrecht 3584 CC (The Netherlands)
[+] These authors contributed equally to this work.
Supporting information and the ORCID identification number(s) for the author(s) of this article can be found under: https://doi.org/10.1002/anie.202013377.

  

on the support. They are also based on Boltzmann single ion thermometry, which limits the maximum relative sensitivity.

Covalent organic frameworks (COFs) are an emerging class of crystalline porous materials, which have already shown massive potential in catalysis, gas adsorption and storage, batteries, and drug delivery.[23–29] Recently, some of us have reported the first lanthanide-grafted COF for white light applications, and shortly afterwards the use of lanthanide-grafted COFs for luminescence thermometry applications, proving its potential also in luminescence applications.[30,31] Reticular chemistry allows predicting and tuning the crystalline structure by thoughtful selection of the molecular building blocks.[32,33] Up to date various two-dimensional (2D) and dimensional (3D) COFs have been synthesized employing three-solvothermal methods and under ambient conditions.[34,35] In this work we investigated a 2D imine TTA-DFP COF prepared from 4,4′,4″-(1,3,5-triazine-2,4,6-triyl) trianiline (TTA) and 2,6-diformylpyridine (DFP).[30] Imine COFs are formed in an imine condensation, in which a C=N bond is formed by condensation of an amine (-$NH_2$) with an aldehyde (-CHO) group. Imine COFs have already shown great prospective for anchoring metal ions and metal complexes, which has been employed both in metal-based heterogeneous catalysis and very recently in luminescence applications.

In this study, to extend the application of lanthanide-grafted imine COFs, we have immobilized the TTA-DFP COF with a mixture of $Eu^{3+}$ and $Tb^{3+}$ β-diketonate complexes at appropriate ratio, as well as $Cu(OAc)_2$, in an attempt to develop a thermometer-based catalyst. We selected $Cu^{2+}$ as the immobilized d-metal and Glaser-type homocoupling of phenylacetylene as a proof-of-principle catalytic reaction. Glaser type coupling reactions are widely known for the synthesis of conjugated diynes and are mainly catalyzed by copper salts ($Cu^{2+}$, $Cu^{+}$) and copper oxide.[36–38] It was observed in this study that the presence of the $Cu^{2+}$ ions strongly affect the temperature-dependent luminescence properties of the lanthanide grafted TTA-DFP COF. Also, the solvent, in which the Eu,Tb@TTA-DFP COF@Cu material is dispersed in, has a huge impact on the ratio of $Eu^{3+}$ to $Tb^{3+}$ emission intensities in the luminescence spectra, significantly affecting the thermometry properties and the relative sensitivity. This is the first time COFs are proposed for this application and, to the best of our knowledge, also the first report where the catalyst and thermometer are reported as one material and not several materials embedded on one platform. Moving toward dual ion thermometry also allows obtaining higher relative sensitivity of the luminescence thermometer.

## Results and Discussion

TTA-DFP COF (Scheme 1) was synthesized following our earlier work by utilizing the dynamic imine condensation reaction.[30] TTA-DFP COF is insoluble in water and in common organic solvents (like diethyl ether, acetone, ethanol, tetrahydrofuran, dioxane, N,N-dimethylformamide, dichloromethane, dimethyl sulfoxide). The powder Cu-$K_\alpha$ X-ray diffraction (PXRD) pattern matches well with the previous report of TTA-DFP COF.[30] A crystalline framework formation is observed with an intense peak at $2\theta = 5°$

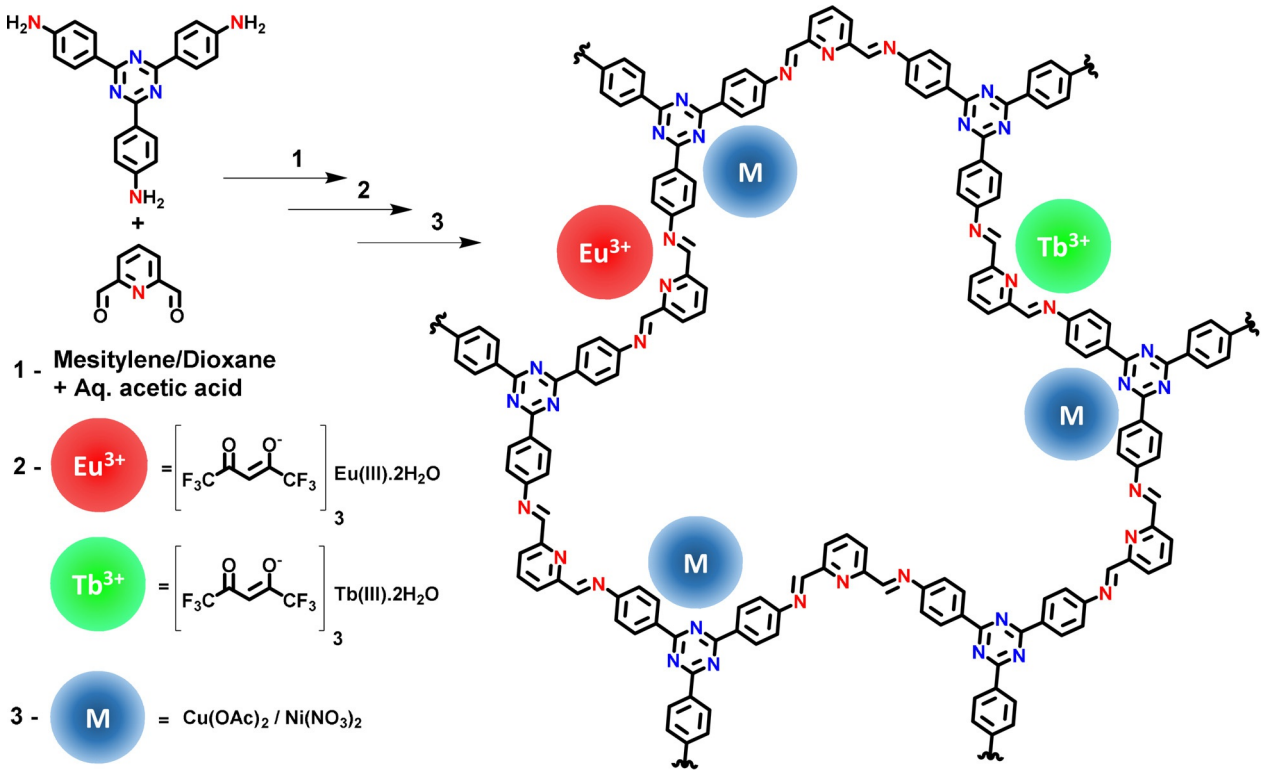


*Scheme 1.* Schematic representation of the TTA-DFP COF and grafting of the lanthanide and d-metal into the framework.

  

corresponding to the (110) plane and a *d*-spacing of 17.6 Å. The reflection from the (003) plane arises from the 2D sheet stacking corresponding to the peak at $2\theta = 25.6°$ (Figure 1 a). An ABC sequence arrangement with unit cell parameters of $a = b = 33.0$ Å and $c = 10.39$ Å and a 2D stacking plane distance of 3.5 Å is obtained as the best match. The PXRD patterns of the material after metal grating have been presented in Figure S1. Upon the addition of the lanthanide complexes and copper acetate, the intensity of the COF (110) peak at 5° is reduced. Such phenomenon has been observed previously in other COFs due to the intercalation of metal ions and other larger moieties to form covalent organic nanosheets through exfoliation. The surface area of activated TTA-DFP COF was evaluated by performing $N_2$ adsorption/desorption isotherms at 77 K. The isotherms of TTA-DFP COF show a reversible type-IV adsorption isotherm (Figure 1 c). The fitting of the data to Brunauer-Emmett-Teller (BET) equation gives rise to a BET specific surface area of 265 $m^2 g^{-1}$.

The formation of the imine bond (C=N) is confirmed by the presence of a stretching band at 1685 $cm^{-1}$ in the FT-IR spectra (Figure 1 b). There are also residual signals due to the unreacted monomers at the edges of the COF. The 2D TTA-DFP COF was further grafted with lanthanide complexes and $Cu^{2+}$ ions in a two-step procedure described in the experimental part. The grafting of the $Ln^{3+}$ ions as well as $Cu^{2+}$ ions is confirmed by nitrogen sorption (Figure 1 b) as well as ICP-MS. After anchoring the TTA-DFP COF with 1 % $Eu(tfac)_3$ and 99 % $Tb(tfac)_3$ complexes (tfac = trifluoroacetylacetone) the BET surface area decreased to 142 $m^2 g^{-1}$. After additional grafting of the Eu,Tb@TTA-DFP COF with $Cu(OAc)_2$ the surface area further dropped to 56 $m^2 g^{-1}$ confirming the anchoring of the metals onto the COF and formation of a Eu,Tb@TTA-DFP COF@Cu material. ICP-MS analysis shows the following metal contents in the sample: 38.2 $mg g^{-1}$ Tb, 0.485 $mg g^{-1}$ Eu and 32.7 $mg g^{-1}$ Cu. Although a much lower amount of $Cu(OAc)_2$ compared to lanthanide ions is used in the synthesis it is clear Cu preferentially binds to the TTA-DFP COF platform.

We further performed TEM analysis on the TTA-DFP COF and TEM and STEM-EDX on the Eu,Tb@TTA-DFP-COF@Cu materials to analyze the morphology (Figure S2,S3) and the distribution of the $Eu^{3+}$, $Tb^{3+}$ and $Cu^{2+}$ ions on the material, respectively (Figure S4,S5). As shown in Figure S2, after anchoring the lanthanide complexes and $Cu(OAc)_2$ there are no changes to the morphology of the TTA-DFP COF (Figure S2), which shows a layered structure. The presence and high dispersion of the metal ions in the Eu,Tb@TTA-DFP COF@Cu sample were confirmed by high angle annular dark-field scanning TEM with the corresponding element maps (C, N, O, Eu, Tb, Cu) obtained by energy dispersive X-ray (EDX) analysis (Figure S3,S4).

The photoluminescence properties of the pristine TTA-DFP COF in solid state were recorded at RT and the combined excitation-emission spectrum has been presented in Figure S6. The maximum of the broad band in excitation spectrum is located around 370 nm, whereas the maximum of the emission spectrum is around 440 nm. The material was further grafted with either $Eu(tfac)_3 \cdot 2H_2O$ or $Tb(tfac)_3 \cdot 2H_2O$, and subsequently $Cu(OAc)_2$.

The photoluminescence properties (excitation, emission and luminescence decay times) of these materials were studied at RT in solid state. In Figure 2 the spectra of Eu@TTA-DFP COF and Eu@TTA-DFP COF@Cu have been presented. Upon excitation around 300 nm, in both materials the characteristic $^5D_0 \rightarrow {}^7F_J$ ($J = 0$-4) transition peaks are observed, confirming the presence of $Eu^{3+}$ ions grafted to the COF material.[39] We observe that in the material additionally co-grafted with $Cu^{2+}$ ions aside from the characteristic $^5D_0 \rightarrow {}^7F_J$ ($J = 0$-4) transition peaks of the $Eu^{3+}$ ions also a broad band around 400–550 nm is present. This can be assigned to the ligand band of the TTA-DFP COF and would suggest that the presence of $Cu^{2+}$ ions caused the $Eu^{3+}$ ions emission to be partially quenched. This theory is further supported by the drop of decay

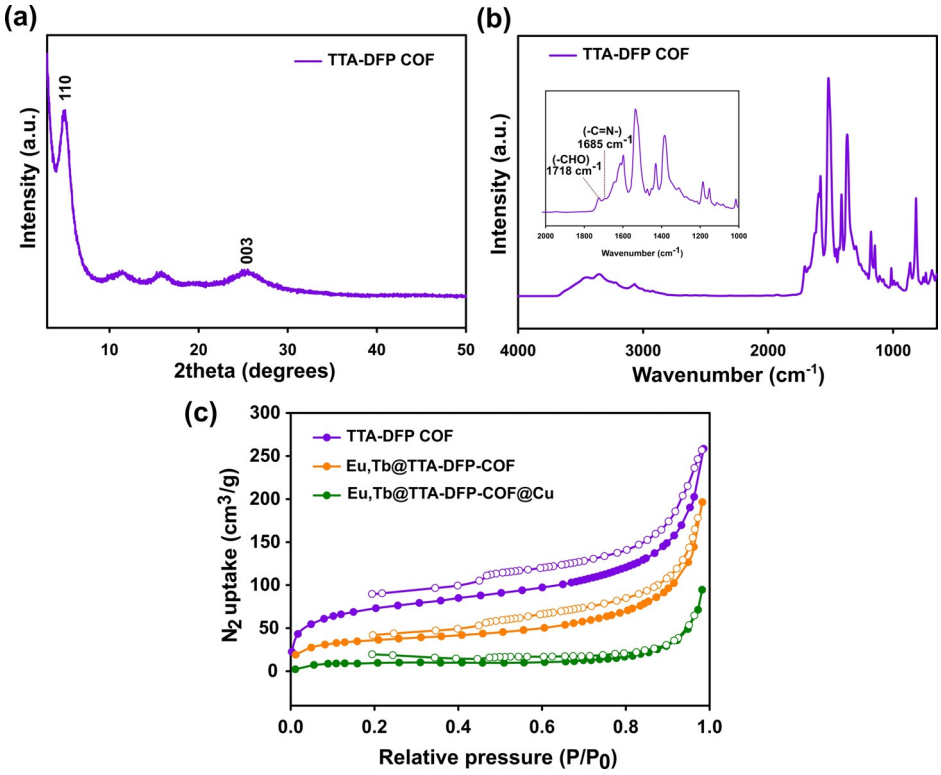


***Figure 1.*** a) PXRD pattern of the TTA-DFP COF, b) FT-IR spectra of TTA-DFP COF; (inset) zoomed region showing imine peaks, c) $N_2$ adsorption/desorption isotherms of TTA-DFP COF (purple), Eu,Tb@TTA-DFP COF (orange), and Eu,Tb@TTA-DFP-COF@Cu (green) at 77 K.

  

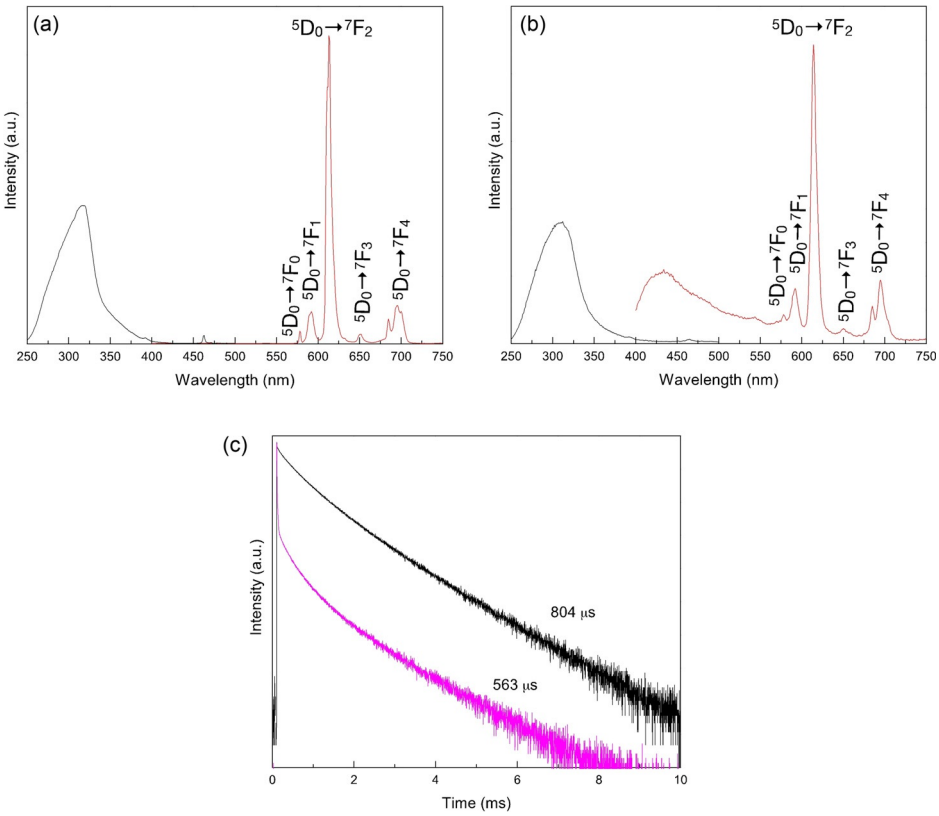


***Figure 2.*** a) RT combined excitation-emission spectrum of Eu@TTA-DFP COF, b) RT combined excitation-emission spectrum of Eu@TTA-DFP COF@Cu, c) luminescence decay times of Eu@TTA-DFP COF (black line) and Eu@TTA-DFP COF@Cu (fuchsia line).

time from 804 µs (before $Cu^{2+}$ grafting) to 563 µs (after $Cu^{2+}$ grafting) dropping to around 70% of the original value. In Figure 3 the spectra of Tb@TTA-DFP COF and Tb@TTA-DFP COF@Cu have been presented. Also in these materials, upon excitation around 300 nm, the characteristic $^5D_4 \rightarrow {}^7F_J$ ($J = 6$-3) transition peaks are observed, confirming the presence of $Tb^{3+}$ ions grafted to the COF material.[40] Similarly as in the Eu-Cu co-grafted materials, also here aside from the characteristic transition peaks of the $Tb^{3+}$ ions also a broad band around 400–500 nm is present. Also in this case a drop in decay time after $Cu^{2+}$ co-grafting is observed (after $Cu^{2+}$ grafting the longer decay time component drops to around 81% of the decay value before $Cu^{2+}$ grafting). Further, a Eu-Tb-Cu co-grafted material was prepared (Figure S7). The Eu-Tb ratio was optimized with the aim of obtaining highest thermometric properties. A ratio of 1% $Eu^{3+}$ to 99% $Tb^{3+}$ was selected and used throughout the whole study.

The possibility of employing the Eu,Tb@TTA-DFP COF compound as a luminescence ratiometric thermometer was investigated. The emission spectra of the compound in solid state were recorded at varying temperatures—from 273–403 K, with a step size of 10 K (−0.15 °C to 129.85 °C, Figure 4a). The integrated areas under the 544 nm and 612 nm peaks have been presented in Figure 4b. It can be observed that the intensity of both peaks decreases with temperature increase, with the 544 nm peak intensity decrease being more pronounced. The $I_{544}/I_{612}$ ratio of the integrated areas under the peaks was calculated (for $Tb^{3+}$: 530–564, for $Eu^{3+}$: 602–630) and these data points could be well fitted employing eqn 1 used for fitting dual-center thermometers, yielding $\Delta_0 = 3.80 \pm 0.39$, $\Delta E = 2170 \pm 163\ cm^{-1}$ and $R^2 = 0.997$.[41,42]

$$\Delta = \frac{\Delta_0}{1 + \alpha \exp\left(-\frac{\Delta E}{k_B T}\right)} \quad (1)$$

Here $\Delta E$ represents the activation energy for thermal quenching of the $Tb^{3+}$ emission, assuming that thermal quenching of the $Eu^{3+}$ emission is negligible. As also some quenching of the $Eu^{3+}$ emission is observed. In this case Equation (1) is still a good approximation and $\Delta E$ can be interpreted as the effective activation energy describing the thermal behavior of the $Tb^{3+}$/$Eu^{3+}$ emission intensity and reflecting the difference in thermal quenching behavior of the green $^5D_4$ emission from $Tb^{3+}$ and the red $^5D_0$ emission from $Eu^{3+}$. The effective activation energy describing the thermal behavior of the $Tb^{3+}$/$Eu^{3+}$ emission intensity reflects the difference in thermal quenching behavior of the green $^5D_4$ emission from $Tb^{3+}$ and the red $^5D_0$ emission from $Eu^{3+}$. Typically, for organic complexes the $Tb^{3+}$ emission is quenched with a lower activation energy due to the higher energy position of the $^5D_4$ level. The good $R^2$ fit obtained when using this equation indicates the presence of only one effective activation energy in this compound. The plot showing the calibration curve for this sample has been presented in Figure 5c. The relative sensitivity value ($S_r$) was calculated employing Equation (2).[43]

$$S_r = 100\% \times \left|\frac{1}{\Delta}\frac{\partial \Delta}{\partial T}\right| \quad (2)$$

$S_r$ indicates the relative change of the thermometric parameter per degree of temperature change (%/°C). The advantage of this parameter is its independence of the nature of the thermometer, which allows direct and quantitative comparison with different materials.[3] The maximum $S_r$ value for this material was calculated to be 2.4%/°C (49.85 °C) (Figure 4d).

The temperature uncertainty $\delta T$ of the compound was calculated using Equation (3) (where $\frac{\delta\Delta}{\Delta}$ is the relative error in the determination of the thermometric parameter) and was shown to be $< 0.4$ °C throughout the whole studied temperature range (Figure 4e).[43]

  

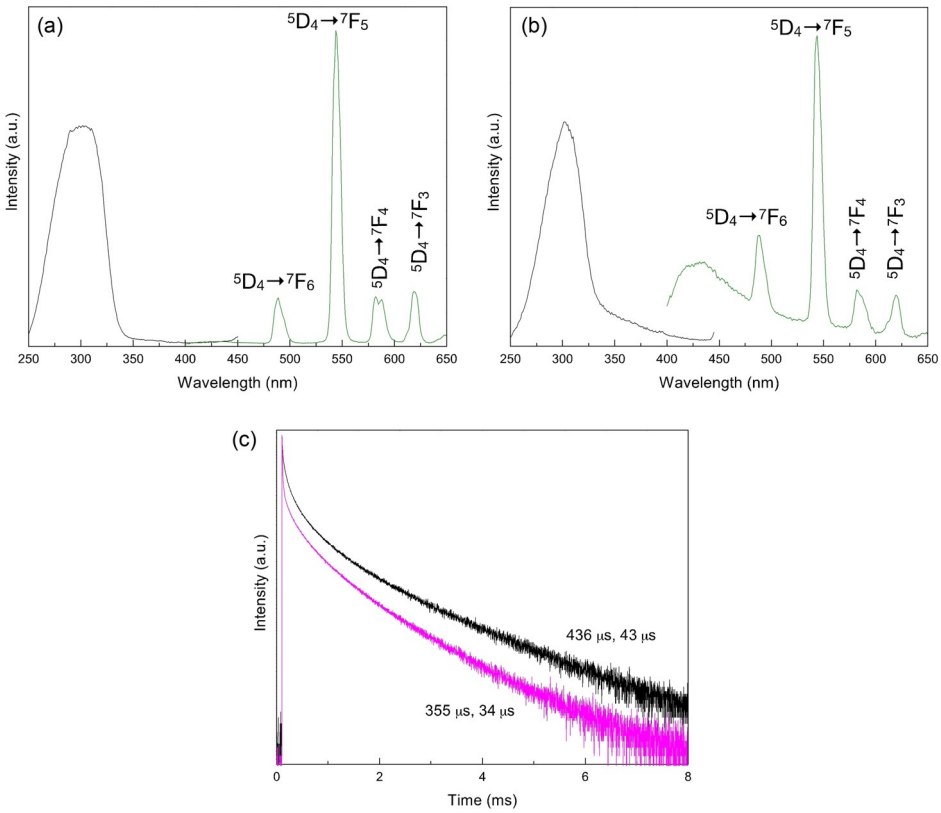


***Figure 3.*** a) RT combined excitation-emission spectrum of Tb@TTA-DFP COF, b) RT combined excitation-emission spectrum of Tb@TTA-DFP COF@Cu, c) luminescence decay times of Tb@TTA-DFP COF (black line) and Tb@TTA-DFP COF@Cu (fuchsia line).

$$\delta T = \frac{1}{S_r}\frac{\delta\Delta}{\Delta} \quad (3)$$

The luminescence and thermometric properties of the Eu,Tb@TTA-DFP COF material were also tested after dispersing them in a polar solvent—ethanol (2 mg COF in 2 mL solvent) (Figure S8). Upon dispersing in ethanol the $Tb^{3+}$ to $Eu^{3+}$ ratio changes indicating a stronger quenching of the $Eu^{3+}$ emission by multi-phonon relaxation because of the high OH vibrational energy and small $^5D_0 \rightarrow {}^7F_6$ gap for $Eu^{3+}$ versus the $^5D_4 \rightarrow {}^7F_0$ gap for $Tb^{3+}$. A slightly higher relative sensitivity (up to 2.7 %/°C) was obtained. This indicates that a solvatochromic effect is observed. Further, the thermometric properties of the Eu,Tb@TTA-DFP COF@Cu compound were studied after dispersing the compound in toluene. 2 mg of the compound were dispersed in 2 mL toluene and an ultrasound bath was used to disperse the compound well in the solvent (Figure 5). The Eu,Tb@TTA-DFP COF@Cu compound was also dispersed in ethanol for comparison (Figure S9,S10).

The presence of $Cu^{2+}$ ions clearly induces an increase in the relative emission intensity between the $Eu^{3+}$ and $Tb^{3+}$ ions compared to the compound before $Cu^{2+}$ grafting. Also in this case, as previously in the Eu,Tb@TTA-DFP COF material, a solvatochromic effect is observed in the polar and nonpolar solvent environment. Dispersion of the material in toluene results in a higher maximum relative sensitivity (4.1 %/°C at 42 °C, see Figure 5c). Also, a very good temperature uncertainty $\delta T < 0.37$ °C was recorded throughout the whole investigated temperature region (293.15–363.15 K; 20–90 °C) and a good reproducibility was observed through cycle tests (Figure S11).

The ability to graft both d-metal and lanthanide ions in one COF material without losing luminescence properties, as well as excellent thermometric properties in this temperature regime, is attractive for many catalytic reactions. Based on the initial luminescence properties of Eu,Tb@TTA-DFP COF@Cu, we were further motivated to study this material as a catalyst, which can simultaneously be employed to measure the temperature for example, inside the reactor. Glaser-type homocoupling of phenylacetylene was selected as the catalytic reaction (Scheme 2). The Glaser type coupling reaction is widely known for the synthesis of conjugated diynes and is mainly catalyzed by copper salts ($Cu^{2+}$, $Cu^{+}$) and oxides.[44] The reaction was selected due to the presence of $Cu^{2+}$ ions on the COF material as well as its excellent thermometric properties in a nonpolar solvent. Toluene was selected as the solvent for carrying out the Glaser reaction as it is an „innocent“ solvent and does not cause metal reduction/oxidation.

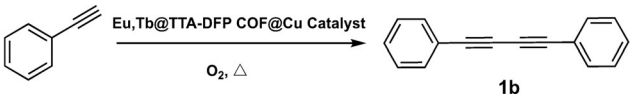


***Scheme 2.*** General reaction Scheme for Glaser coupling reaction.

Although several hypothesis regarding the oxidation state of the Cu-salt and reaction intermediates have been proposed, only very few detailed mechanistic studies have been reported to investigate the Cu-acetylene chemistry.[45,46] Most of the research has been focused only on the substrate scope, different Cu catalysts (homogeneous to heterogeneous) and the nature of the bases and/or additives.[47–50] The use of bases and/or additives additionally hinders the understanding of the mechanism. An ideal case would be to use a heterogeneous catalyst without any base and/or additives, where the structural changes of the homogeneous catalyst during the incoming substrate and the interference of the base and/or additives can be neglected. In Table S1 studies on different type of Cu heterogeneous catalysts have been presented. Among various supports, COFs are considered as promising candidates due to their chemical robustness and tunable

  

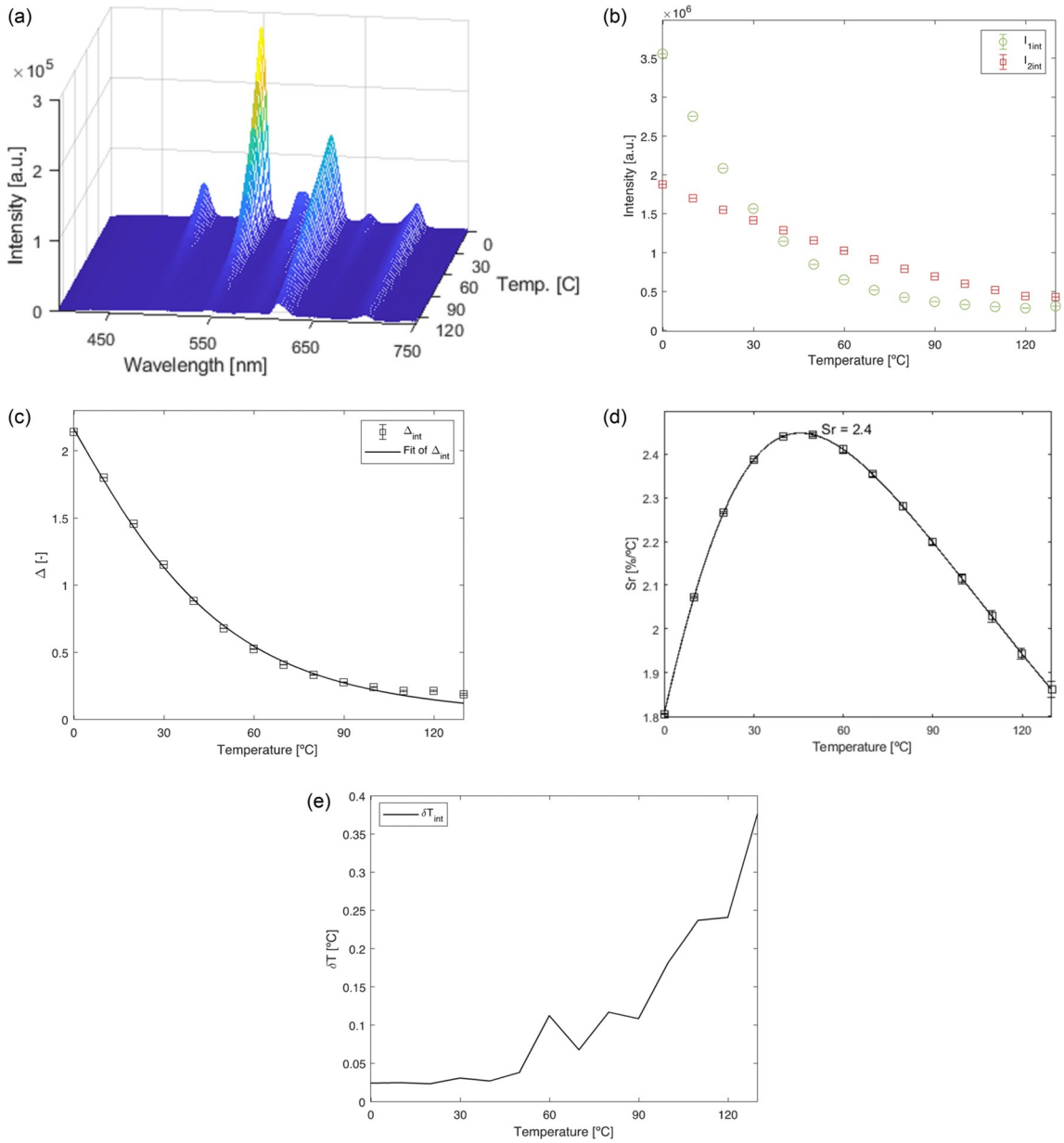


***Figure 4.*** a) Emission map of Eu,Tb@TTA-DFP COF recorded at 273–403 K with step size 10 K (−0.15 °C to 129.85 °C) is solid state form, b) integrated area values for Eu,Tb@TTA-DFP COF as a function of temperature (green squares are shown for the 544 nm values, red circles are shown for the 612 nm values), c) plot presenting the calibration curve for Eu,Tb@TTA-DFP COF when Equation (1) is employed. The points show the experimental delta parameters and the solid line shows the best fit of the experimental points ($R^2 = 0.997$), d) plot presenting the relative sensitivity $S_r$ values at varied temperatures (−0.15 °C to 129.85 °C)) for Eu,Tb@TTA-DFP COF compound. The solid line is a guide for the eyes. e) Temperature uncertainty for Eu,Tb@TTA-DFP COF compound estimated using Equation (3). $\delta T < 0.4$ °C in the whole temperature range.

porous architecture. Recently, Vaidhyanathan et al., reported $Cu/Cu_2O$ nanoparticles supported phenol-pyridyl COF as a heterogeneous catalyst for the synthesis of unsymmetrical alkynes.[51]

Using several spectroscopic and time dependent studies, Corma et al. showed that the $CuO_x$ nanoparticles of size 2 nm and the $CuO_x$-NCs (NCs-nanoclusters) formed in situ during the catalytic reaction (by reduction of $Cu^{2+}$ and $Cu^{+}$ in dimethyl sulfoxide) are the real catalytically active species for homocoupling of diynes.[38,48] It has been observed that CuCl and $CuCl_2$ have the induction period of 1 h and 2 h, respectively, whereas $CuO_x$-NCs had no induction period. To avoid such reduction of Cu salt, we considered toluene as the best innocent solvent for the catalysis. The catalytic reaction was carried out in toluene at 90 °C under air. The time dependent $^1$H NMR studies confirmed that the reaction was completed in 16 h without long induction period. The longer reaction time was quite expected because of the relatively lower surface area of the catalyst, Eu,Tb@TTA-DFP COF@Cu (Figure 1 b). To further test the heterogeneity of the reaction, the catalyst was recycled and used for three cycles and showed same reactivity for the reaction (Fig-

  

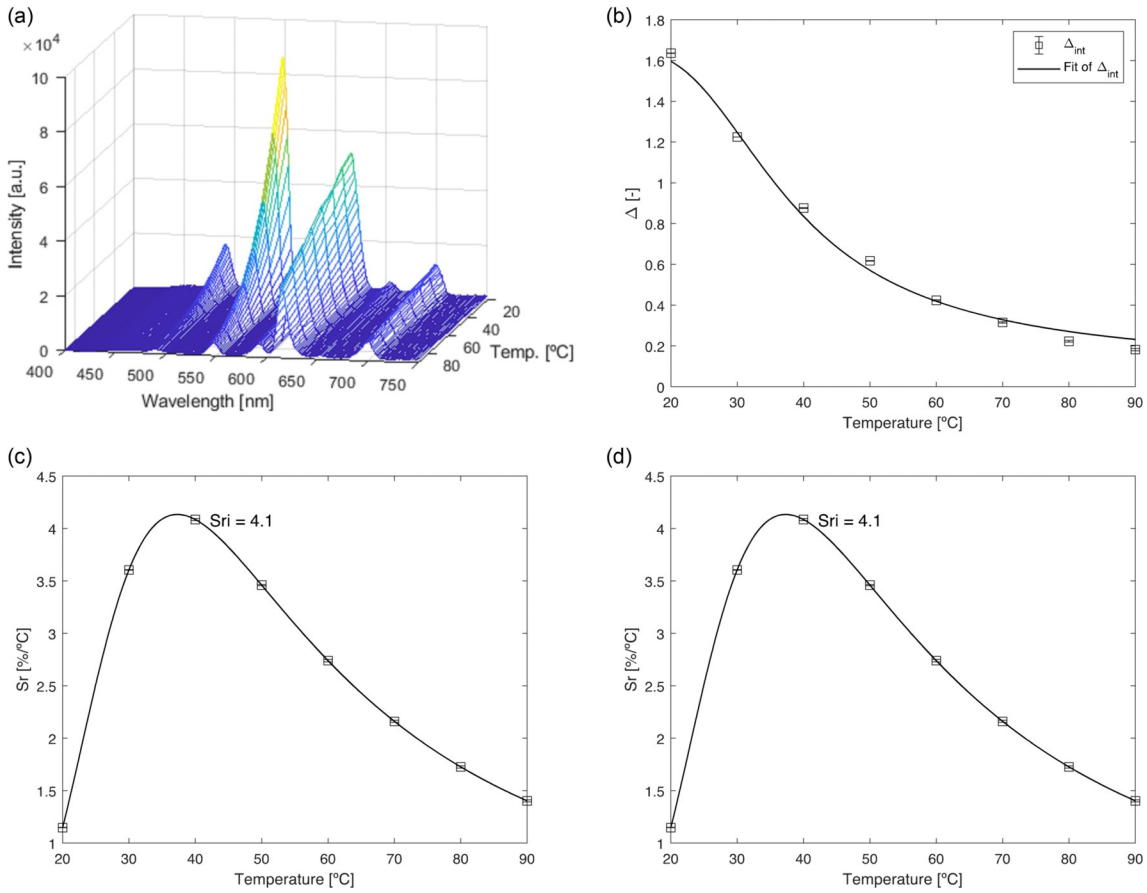


***Figure 5.*** a) Emission map of Eu,Tb@TTA-DFP COF@Cu recorded at 293.15–363.15 K (step size 10 K; 20 °C −90 °C) is toluene, b) plot presenting the calibration curve for Eu,Tb@TTA-DFP COF@Cu when Equation (1) is employed. The points show the experimental delta parameters and the solid line shows the best fit of the experimental points ($R^2 = 0.994$), c) plot presenting the relative sensitivity $S_r$ values at varied temperatures (20 °C −90 °C) for Eu,Tb@TTA-DFP COF@Cu compound measured in toluene. The solid line is a guide for the eyes. d) Temperature uncertainty for Eu,Tb@TTA-DFP COF@Cu compound estimated using Equation (3). $\delta T < 0.37$ °C in the whole temperature range.

ure S12b). A leaching test by hot filtration of the reaction after 6 h was performed and confirmed the absence of leaching during the reactions (Figure S12a). With these results, it was confirmed that the lanthanide-based thermometer could be used as heterogeneous catalyst. Additionally, the observed enhanced catalytic reactivity without base occurs due to the synergistic effect between COF, lanthanides and Cu. In the COF, the imine unit is redox active[51] and hence can easily control the oxidation state of Cu ions during the catalytic reaction. We believe the observed high reactivity is due to the site selective coordination of $Eu^{3+}/Tb^{3+}$ to the triazine-imine sites (imine-N + pyridine-N) and $Cu^{2+}$ to the triazine-Ns (Scheme 1). Furthermore, such coordination help lanthanides to retain their luminescence properties, while Cu performs the catalysis. In order to further confirm the coordination of lanthanides and copper ions to the COFs, XPS analysis was performed. We observed similar shift in binding energy of N 1s from 397.88 eV (TTA-DFP COF) to 399.08 eV (Eu, Tb@TTA-DFP COF) as observed earlier.[30] This confirmed the coordination of lanthanides and copper to the COF. Furthermore, the oxidation state of copper ions in Eu, Tb@TTA-DFP COF@Cu before and after the catalysis were explored. As shown in Figure S13, for Eu, Tb@TTA-DFP COF@Cu before catalysis, binding energies peaks at 934.9 eV and 954.7 eV corresponding to $Cu2p_{3/2}$ and $Cu2p_{1/2}$ respectively and that matches well with the $Cu^{2+}$ ion in CuO. In addition, shake-up satellite peaks between 940–945 eV and 960–965 eV confirmed the presence of $Cu^{2+}$ in the sample before catalysis. In addition, the observed binding energy values at 932.6 eV and 952.4 eV can be assigned to $Cu^{1+}$. The observed $Cu^{1+}$ ions before the catalysis are due to the degradation of $Cu^{2+}$ ions under long X-ray exposure of ion bombardment. However, the decrease in intensities of these satellite peaks in the sample after catalysis confirmed the reduction of $Cu^{2+}$ during the catalytic reactions. The relative reduction of $Cu^{2+}$ ($Cu^{1+}/Cu^{2+} = 2.41$ %; before catalysis) to $Cu^{1+}$ ($Cu^{1+}/Cu^{2+} = 3.72$ %; after catalysis) during the catalysis confirmed the single sites, catalysis and ruled out the formation of any copper NPs or NCs during the reactions. This confirmed that COF with site specific binding sites acts as a smart support to limit the conversion of metal ions to NPs or NCs as seen in other heterogeneous systems.

Further to prove that this material could be simultaneously employed as a catalyst and thermometer, its stability was tested by recording the luminescence after 7 h of heating the material in toluene at 90 °C (Figure S14,S15) and by

  

employing TGA (Figure S16). No significant decrease of luminescence intensity was observed after this heating period. Also, no change in the Eu-to-Tb ratio was observed after the extended heating process indicating the material is stable under the investigated conditions.

As a final proof-of-principle the catalytic reaction was carried out for 20 h and the performance of the Eu,Tb@TTA-DFP COF@Cu material was tested for its luminescence properties without stopping the reaction (Figure 6) at two different temperatures (50 °C and 90 °C). Good luminescence properties were observed for the catalyst and could be observed even with the bare eye when placed under a 302 nm UV lamp (inset Figure 6). The recorded emission spectra were in good agreement with the temperature dependent measurements presented in Figure 5 upon consideration of the Tb-to-Eu ratio of emission intensity at varied temperatures.

Also, NMR analysis proved the formation of the final product (1b) at good yield (Figure S17). Additionally, the material was filtered from the reaction solution after catalysis and investigated using TEM and STEM-EDX (Figure S18–S20). TEM showed no significant changes to the TTA-DFP COF morphology before and after carrying out the reaction. Although it seems like during the reaction the 2D COF sheets separates into single layers. The observed structural changes are due to the incoming reactant (1a) and the outgoing product (1b). Since, both 1a and 1b are planar and rigid, the COF is forced to rearrange itself to retain π-stacking interactions with both the compounds and allow them to diffuse during the catalytic reactions. EDX mapping was carried out to confirm that Eu, Tb and Cu ions were sill grafted on the TTA-DFP COF platform and did not leach out during the reaction. We also investigated whether $CuO_x$ nanoparticles had been formed in the reaction as observed in a previous report. Using HRTEM we did not observe the formation of any $CuO_x$ during the catalytic reaction. By employing luminescence spectroscopy it was not possible to determine if $Cu^I$ is formed during the catalytic synthesis as the spectra of TTA-DFP COF@$Cu^I$ and TTA-DFP COF@$Cu^{II}$ are almost identical and the strong emission band around 400–500 nm originates from the COF material making it difficult to analyze the emission spectra (Figure S21).

These results prove that the Eu,Tb@TTA-DFP COF@Cu material has dual mode function and can be employed simultaneously as a catalyst for the Glaser coupling reaction as well as a luminescent thermometer to measure the temperature in a working environment. This is one of the few reports of combining catalysis with luminescence thermometry, and to the best of our knowledge the only report where the catalyst and thermometer are one material and not several materials embedded on one platform. This concept can be further extended to other d-metals (see SI Figure S22 and S23 for thermometry results using Eu,Tb@TTA-DFP COF@Ni compound, it was observed that also here the presence of the metal and solvents had a significant influence on the thermometry properties and could be used to design a thermometer with performance in the desired temperature and sensitivity range) as well as other COF platforms giving a wide versatility of possible catalytic reactions and thermometric ranges. As we have shown in our previous work the use of LnCOFs for thermometry is even more promising then the very attractive up until now LnMOFs and shows many possibilities for combining research fields such as thermometry with catalysis.[31,52–54]

## Conclusion

In conclusion, in this work we have explored Covalent Organic Frameworks co-grafted with lanthanide ions ($Eu^{3+}$, $Tb^{3+}$) and $Cu^{2+}$, for their synchronous use as a catalyst and nanothermometer in a working environment. Such a material could be an excellent solution for the accurate monitoring of temperature non-invasively in different regions of a catalytic reactor to ensure temperature homogeneity. This is the first time COFs are proposed for this application, and to the best

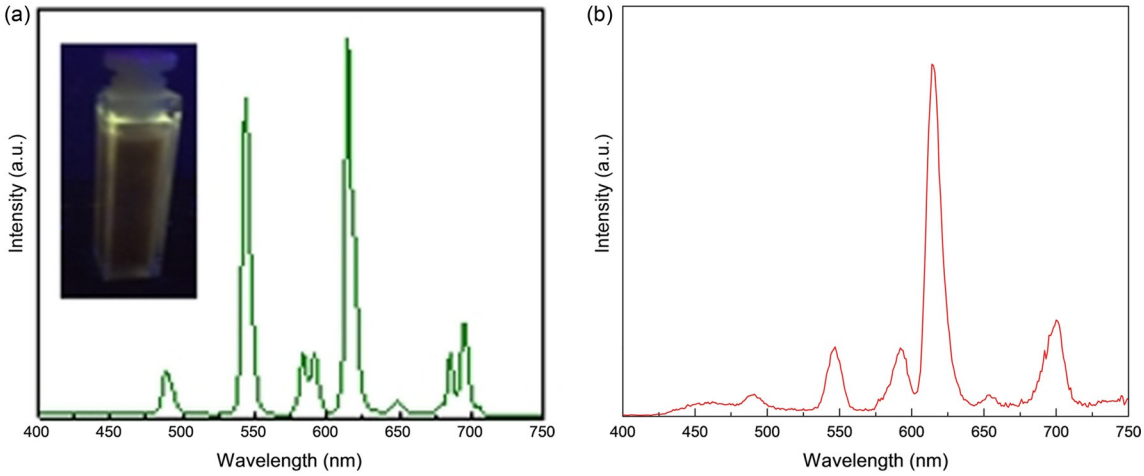


*Figure 6.* a) Emission spectrum of Eu,Tb@TTA-DFP COF@Cu recorded at 50 °C during carrying out the Glaser coupling reaction. The inset shows the catalyst under 302 nm UV lamp in the reaction medium after 20 h of performance. b) Emission spectrum of Eu,Tb@TTA-DFP COF@Cu recorded at 90 °C during carrying out the Glaser coupling reaction.

  

of our knowledge this is also the first report where the catalyst and thermometer are reported as one material and not separate materials embedded on one platform. For a proof-of-principle the Glaser coupling reaction was investigated and the luminescence was investigated in a working environment during the catalytic reaction. Good luminescence signal was obtained, allowing determination of the reaction temperature using luminescence thermometry. We showed that this concept could be potentially extended to other catalytic reactions by grafting other d-metal ions on the platform. Interestingly, we observed that the presence of the d-metal as well as the presence of the different investigated polar and nonpolar solvents affects the thermometric properties of the nanothermometer allowing tunability through these modifications.

## Acknowledgements

A.M.K. acknowledges Ghent University, FWO and BOF (BOF/STA/202002/004) for funding. C.K. acknowledges the support from the Research Board of Ghent University (GOA010-17, BOF GOA2017000303). H.S.J. thanks FWO (PEGASUS)[2] Marie Sklodowska-Curie Grant 665501.

## Conflict of interest

The authors declare no conflict of interest.

**Stichwörter:** catalysis · covalent organic frameworks · Glaser coupling reaction · lanthanides · ratiometric thermometers

[1] R. G. Geitenbeek, A.-E. Niewelink, T. S. Jacobs, B. B. V. Salzmann, J. Goetze, A. Meijerink, B. M. Weckhuysen, *ACS Catal.* **2018**, *8*, 2397.
[2] R. G. Gietenbeek, P. T. Prins, W. Albrecht, A. van Blaaderen, B. M. Weckhuysen, A. Meijerink, *J. Phys. Chem. C* **2017**, *121*, 3501.
[3] L. D. Carlos, F. Palacio, *Thermometry at the Nanoscale: Techniques and Selected Applications.* Royal Society of Chemistry, Oxfordshire, **2016**.
[4] D. Jaque, F. Vetrone, *Nanoscale* **2012**, *4*, 4301.
[5] Z. Wang, D. Ananias, A. Carne-Sanchez, C. D. S. Brites, I. Imaz, D. Maspoch, J. Rocha, L. D. Carlos, *Adv. Funct. Mater.* **2015**, *25*, 2824.
[6] D. Wawrzynczyk, A. Bednarkiewicz, M. Nyk, W. Strek, M. Samoc, *Nanoscale* **2012**, *4*, 6959.
[7] D. Ananias, F. A. Almeida Paz, D. S. Yufit, L. D. Carlos, J. Rocha, *J. Am. Chem. Soc.* **2015**, *137*, 3051.
[8] X.-d. Wang, O. S. Wolfbeis, R. J. Meier, *Chem. Soc. Rev.* **2013**, *42*, 7834.
[9] R. G. Geitenbeek, B. B. V. Salzmann, A.-E. Nieuwelink, A. Meijerink, B. M. Weckhuysen, *Chem. Eng. Sci.* **2019**, *198*, 235.
[10] T. Hartman, R. G. Geitenbeek, G. T. Whiting, B. M. Weckhuysen, *Nat. Catal.* **2019**, *2*, 986.
[11] I. K. van Ravenhorst, R. G. Geitenbeek, M. J. van der Eerden, J. Tijn van Omme, H. H. Perez Garza, F. Meirer, A. Meijerink, B. M. Weckhuysen, *ChemCatChem* **2019**, *11*, 5505.
[12] T. Hartman, R. G. Geitenbeek, C. S. Wondergem, W. van der Stam, B. M. Weckhuysen, *ACS Nano* **2020**, *14*, 3725.
[13] A. Nadort, J. Zhao, E. M. Goldys, *Nanoscale* **2016**, *8*, 13099.
[14] T. Rinkel, A. Naduvilddathu Raj, S. Duhnen, M. Haase, *Angew. Chem. Int. Ed.* **2016**, *55*, 1164; *Angew. Chem.* **2016**, *128*, 1177.
[15] C. Homann, L. Krukewitt, F. Frenzel, B. Grauel, C. Wurth, U. Resch-Genger, M. Haase, *Angew. Chem. Int. Ed.* **2018**, *57*, 8765; *Angew. Chem.* **2018**, *130*, 8901.
[16] D. T. Kliert, M. U. Kumke, *RSC Adv.* **2015**, *5*, 67149.
[17] M. Runowski, N. Stopikowska, D. Szeremeta, S. Goderski, M. Skwierczynska, S. Lis, *ACS Appl. Mater. Interfaces* **2019**, *11*, 13389.
[18] Q. Qiang, Y. Wang, *Front. Chem.* **2019**, *7*, 425.
[19] W. Xu, Y. Hu, L. Zheng, Z. Zhang, W. Cao, *J. Lumin.* **2019**, *215*, 116617.
[20] J. Liu, R. Van Deun, A. M. Kaczmarek, *Nanomaterials* **2019**, *9*, 646.
[21] A. Ćirić, J. Aleksić, T. Barudžija, Z. Antić, V. Đorđević, M. Medić, J. Periša, I. Zeković, M. Mitrić, M. D. Dramićanin, *Nanomaterials* **2020**, *10*, 627.
[22] A. M. Kaczmarek, M. Suta, H. Rijckaert, A. Abalymov, I. Van Driesche, A. G. Skirtach, A. Meijerink, P. Van Der Voort, *Adv. Funct. Mater.* **2020**, *30*, 2003101.
[23] C. S. Diercks, O. M. Yaghi, *Science* **2017**, *355*, eaal1585.
[24] Y. Zheng, R. Zou, Y. Zhao, *Adv. Mater.* **2016**, *28*, 2855.
[25] Y. Zhi, Z. Li, X. Feng, H. Xia, Y. Zhang, Z. Shi, Y. Mu, Z. Liu, *J. Mater. Chem. A* **2017**, *5*, 22933.
[26] S. Lu, Y. Hu, S. Wan, R. McCaffrey, Y. Jin, H. Gu, W. Zhang, *J. Am. Chem. Soc.* **2017**, *139*, 17082.
[27] Y. Du, H. Yang, J. M. Whitley, S. Wan, Y. Jin, S. H. Lee, W. Zhang, *Angew. Chem. Int. Ed.* **2016**, *55*, 1737; *Angew. Chem.* **2016**, *128*, 1769.
[28] S. Wang, Q. Wang, P. Shao, Y. Han, X. Gao, L. Ma, S. Yuan, X. Ma, J. Zhou, X. Feng, B. Wang, *J. Am. Chem. Soc.* **2017**, *139*, 4258.
[29] S. Mitra, H. S. Sasmal, T. Kundu, S. Kandambeth, K. Illath, D. Diaz Dias, R. Banerjee, *J. Am. Chem. Soc.* **2017**, *139*, 4513.
[30] C. Krishnaraj, A. M. Kaczmarek, H. Sekhar Jena, K. Leus, N. Chaoui, J. Schmidt, R. Van Deun, P. Van Der Voort, *ACS Appl. Mater. Interfaces* **2019**, *11*, 27343.
[31] A. M. Kaczmarek, Y.-Y. Liu, M. K. Kaczmarek, H. Liu, F. Artizzu, L. D. Carlos, P. Van Der Voort, *Angew. Chem. Int. Ed.* **2020**, *59*, 1932; *Angew. Chem.* **2020**, *132*, 1948.
[32] S. Das, P. Heasman, T. Ben, S. Qiu, *Chem. Rev.* **2017**, *117*, 1515.
[33] X. Feng, L. Chen, Y. Honsho, O. Saengsawang, L. Liu, L. Wang, A. Saeki, S. Irle, S. Seki, Y. Dong, D. Jiang, *Adv. Mater.* **2012**, *24*, 3026.
[34] F. J. Uribe-Romo, J. R. Hunt, H. Furukawa, C. Klock, M. O'Keeffe, O. M. Yaghi, *J. Am. Chem. Soc.* **2009**, *131*, 4570.
[35] S.-Y. Ding, X.-H. Cui, J. Feng, G. Lu, W. Wang, *Chem. Commun.* **2017**, *53*, 11956.
[36] B. Lai, Z. Huang, Z. Jia, R. Bai, Y. Gu, *Catal. Sci. Technol.* **2016**, *6*, 1810.
[37] A. Sagadevan, V. P. Charpe, K. C. Hwang, *Catal. Sci. Technol.* **2016**, *6*, 7688.
[38] L. Liu, T. Matsushita, P. Concepcion, A. Leyva-Perez, A. Corma, *ACS Catal.* **2016**, *6*, 2211.
[39] A. M. Kaczmarek, Y.-Y. Liu, C. Wang, B. Laforce, L. Vincze, P. Van Der Voort, R. Van Deun, *Dalton Trans.* **2017**, *46*, 12717.
[40] A. M. Kaczmarek, K. Van Hecke, R. Van Deun, *Inorg. Chem.* **2017**, *56*, 3190.
[41] H. Rijckaert, A. M. Kaczmarek, *Chem. Commun.* **2020**, *56*, 14365.
[42] J. K. Zaręba, M. Nyk, J. Janczak, M. Samoć, *ACS Appl. Mater. Interfaces* **2019**, *11*, 10435.
[43] C. D. S. Brites, S. Balabhadra, L. D. Carlos, *Adv. Opt. Mater.* **2018**, 1801239.
[44] J. Liu, J. W. Lam, B. Z. Tang, *Chem. Rev.* **2009**, *109*, 5799.
[45] P. Siemsen, R. C. Livingston, F. Diederich, *Angew. Chem. Int. Ed.* **2000**, *39*, 2632; *Angew. Chem.* **2000**, *112*, 2740.

  

[46] J. Jover, P. Spuhler, L. Zhao, C. Mcardle, F. Maseras, *Catal. Sci. Technol.* **2014**, *4*, 4200.
[47] X. Jia, K. Yin, C. ji, J. Li, H. Bian, *Green Chem.* **2011**, *13*, 2175.
[48] F. Alonso, T. Melkonian, Y. Moglie, M. Yus, *Eur. J. Org. Chem.* **2011**, 2524.
[49] S. Biswas, K. Mullick, S.-Y. Chen, D. A. Kriz, M. D. Shakil, C.-H. Kuo, A. M. Angeles-Boza, A. R. Rossi, S. L. Suib, *ACS Catal.* **2016**, *6*, 5069.
[50] H. Xu, K. Wu, J. Tian, L. Zhu, X. Yao, *Green Chem.* **2018**, *20*, 793.
[51] D. Chakraborty, S. Nandi, D. Mullangi, S. Haldar, C. P. Vinod, R. Vaidhyanathan, *ACS Appl. Mater. Interfaces* **2019**, *11*, 15670.
[52] Y. Cui, H. Xu, Y. Yue, Z. Guo, J. Yu, Z. Chen, J. Gao, Y. Yang, G. Qian, B. Chen, *J. Am. Chem. Soc.* **2012**, *134*, 3979.
[53] X. Rao, T. Song, J. Gao, Y. Cui, Y. Yang, C. Wu, B. Chen, G. Qian, *J. Am. Chem. Soc.* **2013**, *135*, 15559.
[54] X. Liu, S. Akerboom, M. de Jong, I. Mutikainen, S. Tanase, A. Meijerink, E. Bouwman, *Inorg. Chem.* **2015**, *54*, 11323.

Manuskript erhalten: 4. Oktober 2020
Veränderte Fassung erhalten: 2. November 2020
Akzeptierte Fassung online: 10. November 2020
Endgültige Fassung online: 15. Dezember 2020

  